Cellular/Molecular

Kv7/KCNQ Channels Control Action Potential Phasing of Pyramidal Neurons during Hippocampal Gamma Oscillations *In Vitro*

Richardson N. Leão, Hui Min Tan, and André Fisahn
Neuronal Oscillations Laboratory, Department of Neuroscience, Karolinska Institute, 17177 Stockholm, Sweden

While the synaptic mechanisms involved in the generation of *in vitro* network oscillations have been widely studied, little is known about the importance of voltage-gated currents during such activity. Here we study the role of the M-current (I_M) in the modulation of network oscillations in the gamma-frequency range (20 – 80 Hz). Kv7/KCNQ subunits, the molecular correlates of I_M, are abundantly expressed in CA1 and CA3 pyramidal neurons, and I_M is an important modulator of pyramidal neuron firing. Using hippocampal slices, we recorded field activity and pyramidal neuron action potential timing during kainate-induced gamma oscillations. Application of the specific I_M blocker XE991 causes a significant reduction of gamma oscillation amplitude with no significant change in oscillation frequency. Concomitant CA3 pyramidal neuron recordings show a significant increase in action potential frequency during ongoing gamma oscillations after the application of XE991. This increase is associated with a significant loss of periodicity of pyramidal neuron action potentials relative to the phase of the gamma oscillations. Using dynamic clamp, we show that I_M acts to improve the periodicity of action potential timing and to decrease action potential frequency. We further validate these results in a compartmental model of a pyramidal neuron. Our work suggests that I_M modulates gamma oscillations by regulating the phasing of action potential firing in pyramidal neurons.

Introduction

Acute brain slice preparations can provide reduced but highly accessible models of neural networks of higher order. The ability to induce gamma oscillations in brain slices (Fisahn et al., 1998) has allowed a dissection of the neural mechanisms involved in the generation of oscillatory patterns (Fisahn, 2005). Cholinergically induced *in vitro* gamma oscillations show several features that are observed in *in vivo* intrahippocampal gamma oscillations (e.g., pyramidal neurons fire at low rates but phase locked to the oscillation, rhythm is generated in area CA3 and propagates to CA1, etc.) (Mann and Paulsen, 2005). Gamma oscillations can also be induced by activation of kainate receptors, and the resulting rhythmic activity seems to involve synaptic mechanisms similar to cholinergically induced oscillations (Traub et al., 2002; Fisahn et al., 2004). While several previous studies have focused on the role of synaptic activity and neural connectivity in the generation of gamma rhythms *in vitro* (Fisahn et al., 2004; Mann et al., 2005; Oren et al., 2006), fewer studies addressed the importance of subcellular mechanisms, in particular K^+ currents, for the modulation of gamma oscillations (Fisahn et al., 2002).

Received March 27, 2009; revised Aug. 7, 2009; accepted Aug. 11, 2009.

This work was supported by a Long-Term Fellowship from the International Human Frontier Science Program Organization awarded to R.N.L., an A*STAR Studentship award to H.M.T., and by the Karolinska Institute, the Swedish Research Council, and the European Commission Coordination Action ENINET (contract number LSHM-CT-2005-19063; A.F.). We thank Prof. J. Storm and Dr. J. Lawrence for critical comments on earlier versions of this manuscript.

Correspondence should be addressed to Dr. André Fisahn, Nobel Institute for Neurophysiology, Department of Neuroscience, Retzius väg 8, A3:5, Karolinska Institute, 17177 Stockholm, Sweden. E-mail: andre.fisahn@ki.se.

DOI:10.1523/JNEUROSCI.1463-09.2009

 0270-6474/09/2913353-12$15.00/0

Together with the hyperpolarization-activated current (I_h), the M-current (I_M) is a prime candidate for a subcellular mechanism capable of modulating network synchrony. The M-current is a slowly activating and non-inactivating voltage-dependent K^+ current abundantly expressed in hippocampal pyramidal neurons (Halliwell and Adams, 1982; Pedarzani and Storm, 1995). In the hippocampus, perisomatic I_M is known to control the excitability of pyramidal neurons (Gu et al., 2005; Yue and Yaari, 2006) and blocking I_M in CA3 pyramidal neurons acts to increase action potential (AP) afterdepolarization and promotes burst firing (Vervaeke et al., 2006). Recently an increasing number of studies has focused on I_M, as a new generation of antiepileptic and cognitive-enhancing drugs targeting this current became available. However, I_M is present in numerous different brain nuclei and its role in network function is complex and poorly understood. A global attenuation or augmentation of I_M to treat conditions that affect particular brain areas may cause unwanted effects in nonaffected regions and attempts to improve cognition using I_M blockers largely failed, underscoring our lack of understanding of I_M function. For example, linopirdine, an I_M blocker and a neurotransmitter release enhancer, appeared to be a promising therapeutic agent for memory deficits a decade ago (Lamas et al., 1997) but failed to deliver meaningful results in clinical trials (Rockwood et al., 1997; Börjesson et al., 1999). Another more potent I_M blocker and neurotransmitter release enhancer, XE991 [10,10-bis(4-pyridinylmethyl)-9(10*H*)-anthracenone], is currently undergoing clinical trials, with no significant results obtained so far (Romero et al., 2004). To understand the discrepancy between the known effects of I_M on the cellular level and the apparent ineffectiveness of therapies targeting I_M it is fundamen-

tal to address its role in cognition-relevant activity in local networks. Here we demonstrate that kainate-induced gamma oscillation in hippocampal slices are reduced by I_M antagonists as a result of decreased phase coupling of CA3 pyramidal neuron APs when Kv7/KCNQ channels are blocked. Furthermore, we show that selective restoration of I_M in single pyramidal neurons by dynamic clamp (DC) increases AP phase coupling back to control levels.

Materials and Methods

Electrophysiology. Electrophysiological experiments were performed in hippocampal slices of Sprague Dawley rats (postnatal day 21–24). All procedures followed Swedish and Karolinska Institute guidelines for the care and use of laboratory animals. Rats were decapitated and the brains rapidly removed and placed in ice-cold artificial CSF (ACSF) containing the following (in mM): 2.49 KCl, 1.43 NaH_2PO_4, 26 $NaHCO_3$, 10 glucose, 252 sucrose, 1 $CaCl_2$, 4 $MgCl_2$. The brain was then hemisected and trimmed and horizontal 400-μm-thick hippocampal slices were obtained using a vibratome. Slices were kept in a submerged holding chamber containing ACSF (in mM: 124 NaCl, 3.5 KCl, 1.25 NaH_2PO_4, 1.5 $MgCl_2$, 1.5 $CaCl_2$, 30 $NaHCO_3$, 10 glucose), constantly bubbled with 95% O_2 and 5% CO_2, incubated at 35°C for 1 h, and then allowed to cool to room temperature. For recordings, slices were transferred to a submerged recording chamber (28°C) under an upright microscope equipped with infrared and differential interference contrast optics and perfused with oxygenated ACSF at a rate of 1–1.25 ml/min. We opt for the usage of a submerged chamber rather than an interface chamber to be able to perform patch-clamp recordings from cells under visual guidance. While oscillations have a better signal-to-noise ratio in interface chambers, there are no differences in oscillation frequency and in pyramidal neuron firing (Fisahn et al., 2004). The differences in power observed between submerged versus interface recording chambers appear to reflect different oxygenation levels but synaptic transmission is not significantly different between the two recording configurations (Hájos et al., 2009). Extracellular field and intracellular whole-cell patch-clamp recordings were performed using either a Multiclamp 200B or an Axopatch 200B and an Axoclamp 2A amplifier (Molecular Devices). Glass pipettes with tip resistances between 3 and 5MΩ were used. Data were digitized using WinWCP (Dr. John Dempster, http://spider.science.strath.ac.uk/sipbs/software_ses.htm) or a custom acquisition software developed in LabView (National Instruments) and analyzed in Matlab (Mathworks). Extracellular field recordings were made in stratum radiatum of the hippocampal area CA3 and whole-cell patch-clamp recordings from somata of pyramidal neurons of area CA3 as described previously (Fisahn et al., 2002). For field and cell-attached recordings pipettes were filled with ACSF and, for whole-cell patch-clamp recordings, with a K-gluconate-based internal solution (in mM: 17.5 KCl, 122.5 K-gluconate, 9 NaCl, 1 $MgCl_2$, 3 Mg-ATP, 0.3 GTP-Tris, 1 HEPES, 0.2 EGTA; pH was adjusted to 7.2 using KOH). Linopirdine, ZD7288, XE991, and tetrodotoxin were purchased from Tocris Bioscience.

Analysis. Fast Fourier transformations for power spectra were computed from 120-s-long data traces and gamma oscillation power was measured as the integrated power spectra between 20 and 80 Hz. The low cutoff frequency of 20 Hz was chosen because of the low recording temperature (28°C) used in our experiments (at this temperature M-current traces could be fit with a single exponential; see Results). It has been demonstrated that the frequency of gamma oscillations decreases by 3.3 Hz for each 1°C temperature decrease (Dickinson et al., 2003; Fisahn et al., 2009). The phase of APs with regard to field oscillation cycle was analyzed using a template-based algorithm for field cycles (Clements and Bekkers, 1997) and a derivative threshold-based algorithm for detecting action potentials. AP-phase histograms were fitted with third-order polynomial functions as follows:

$$y = ax^3 + bx^2 + cx + d, \quad (1)$$

and the third-order coefficient a used as a measure of the histogram "peakedness" (AP synchronicity or randomness). Data values are reported as means ± SEM. Student's paired t test was used for statistics unless otherwise stated.

Dynamic clamp. To assess the functional effects of the M-current in CA3 pyramidal neurons during gamma oscillations, we have simulated I_M in pyramidal neurons using the dynamic clamp technique. This method was implemented on a second computer running a Linux kernel modified by the Real Time Application Interface for Linux from the Politecnico di Milano Institute-Dipartimento di Ingegneria Aerospaziale (http://www.rtai.org) and custom-made software that reads membrane voltage and generates current commands at a 40 kHz refresh rate using a Data Acquisition data card (National Instruments) and drivers from the Linux Control And Measurement Device Interface (COMEDI, www.comedi.org) (Leao et al., 2005). To block the native I_M of single cells we supplemented our internal solution with 0.5 mM $BaCl_2$ (Lamas et al., 1997). We used $BaCl_2$ instead of XE991 in our internal solution since XE991 did not block I_M significantly (even at high concentrations of 40 μM; data not shown). Our non-inactivating I_M model followed a Hodgkin and Huxley notation, i.e., $I_M = \bar{g}_M u(V - V_K)$, where $\bar{g}_M$ is the maximal I_M conductance, V is the membrane voltage, and V_K is the K^+ reversal potential. The evolution variable u was numerically solved using the following equation:

$$\frac{du}{dt} = \frac{u_\infty(V) - u}{\tau_u(V)}. \quad (2)$$

The kinetic functions of our model [$\tau_u(V)$ and $u_\infty(V)$] were constructed from the time constants-versus-voltage and current-versus-voltage relationships of XE991-sensitive current traces. Time constants for each voltage step were obtained by fitting the XE991-sensitive currents with single exponentials and time constants-versus-voltage relationships were fitted with a function of the following form:

$$\tau_u(V) = \frac{SF}{C_a e^{V_a(V+V_c)} + C_b e^{V_b(V+V_c)}} + M \quad \tau_u(V) = \frac{SF}{C_a e^{V_a(V+V_c)} + C_b e^{V_b(V+V_c)}} + M. \quad (3)$$

The normalized conductance $g_M/\bar{g}_M$ versus voltage relationship, where $\bar{g}_M$ is the maximum conductance and $g_M = I_M (V - V_K)$, the 20 μM XE991-sensitive M-current, was fitted with the following function:

$$g/\bar{g} = (1 + e^{-(V+V_{1/2})/k})^{-1}. \quad (4)$$

The results of the least-square fit of these functions are shown in Results.

Modeling. We also tested the importance of I_M in a pyramidal neuron model based on the modified Pinsky–Rinzel model (Pinsky and Rinzel, 1994) as implemented by Tiesinga et al. (2001). A pyramidal neuron consisted of a soma with voltage equal V_S and a single dendritic compartment with voltage equal to V_D. All voltage-gated currents except I_M were implemented according to Tiesinga et al. (2001) as follows:

$$C_M \frac{dV_S}{dt} = -g_L(V_S - E_L) - I_{Na} - I_{KDR} - I_M - \frac{1}{2} g_c(V_S - V_D) \quad (5)$$

and

$$C_M \frac{dV_D}{dt} = -g_L(V_S - E_L) - I_{Ca} - I_{KAHP} - I_{KC} - I_{NaO} - I_{KO} - I_{syn} - \frac{1}{2} g_c(V_S - V_D), \quad (6)$$

where g_L is the leak conductance, E_L is the leak reversal potential, I_{KDR} is a delayed-rectifier potassium current, a fast sodium I_{Na}, and the "coupling current" between the dendrite and soma compartments. The dendrite voltage was determined by calcium current I_{Ca}, afterhyperpolarization (AHP) potassium current I_{KAHP}, calcium-dependent potas-

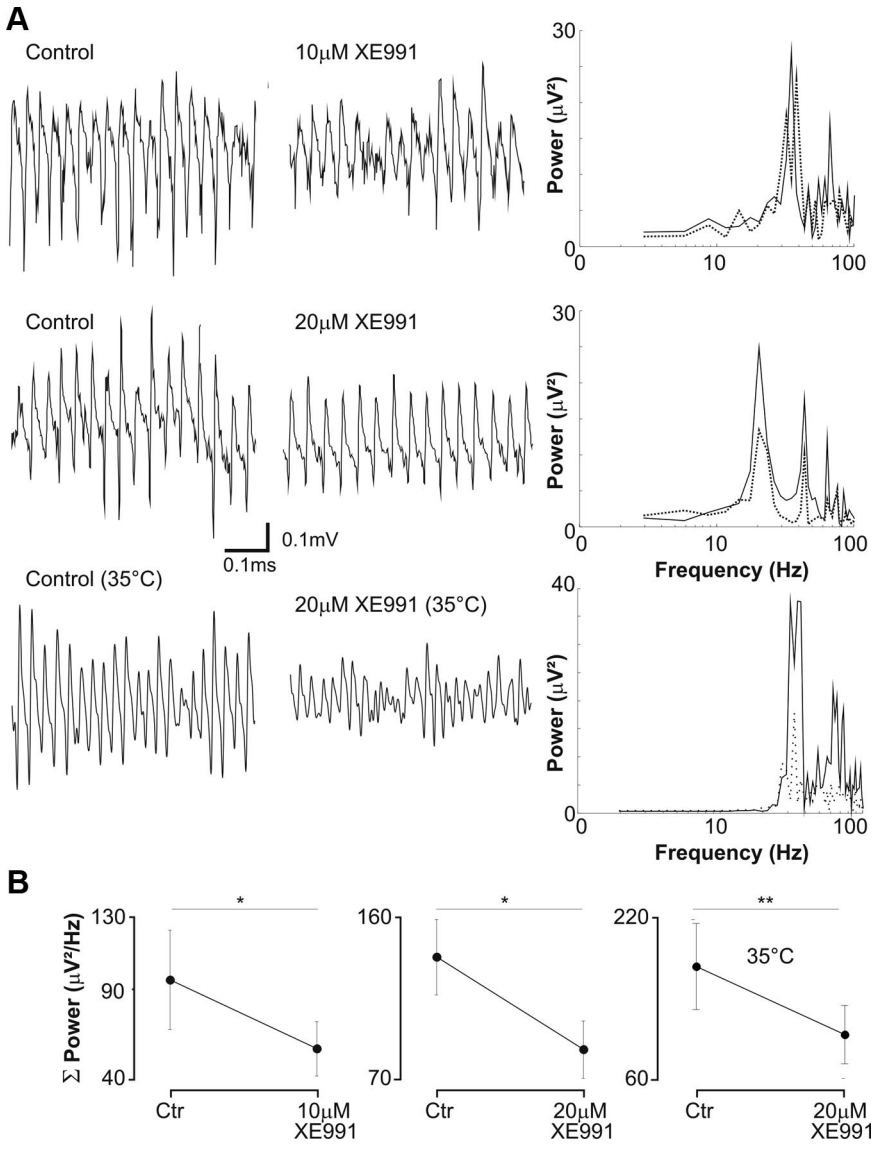

Figure 1. XE991 decreases gamma oscillation amplitude. ***A***, Representative examples of field recordings from hippocampal slices in the presence of 100 nM kainate. Left, Control recordings of kainate-induced gamma oscillations; middle, field activity of the same slices in the presence of 10 or 20 μM XE991 or 20 μM XE991 when the bath temperature was 35°C; right, respective power spectra (solid lines: control; dotted lines: XE991). ***B***, Summary of integrated gamma oscillation power in control conditions and after the application of 10 or 20 μM XE991 or 20 μM XE991 in experiments performed at 35°C. *$p < 0.03$, **$p = 0.04$.

sium current I_{KC}, persistent sodium I_{NaO} and potassium I_{KO} currents, and a leak current. For the implementation of the M-current we used our own experimental results (see above) and placed that current in the somatic compartment. Details for the model implementation and parameter values can be found in the study by Tiesinga et al. (2001). The dendritic compartment also received 10 excitatory inputs and the soma was innervated by 5 inhibitory inputs modeled by α functions ($x_{syn} = t_{syn} e^{(1-t_{syn})/t_p} t_p^{-1}$, $t_{syn} = t_e, t_i$) with a time constant t_p ($t_e = 0.15$ ms for excitatory and $t_i = 0.5$ ms for inhibitory synapses) and t_{syn} as the time of the last synaptic event (t_e and t_i, excitatory and inhibitory times, respectively). Synaptic currents I_{syn} (I_e, excitatory; I_i, inhibitory) were modeled by the following equation: $I_{syn} = \bar{g}_{syn} x_{syn}(V - V_{syn})$, $I_{syn} = I_e, I_i$, $V_{syn} = V_e, V_i$, $\bar{g}_{syn} = \bar{g}_e, \bar{g}_i$, where V_{syn} is the reversal potential for the excitatory ($V_e = 0$ mV) and inhibitory ($V_i = -75$ mV) synapses and $\bar{g}_{syn}$ is the total synaptic conductance ($g_e = 0.05$ ns and $g_i = 0.075$ ns for excitatory and inhibitory synapses, respectively). Rhythmic inputs were modeled by a sinusoid function of 30 Hz frequency that determined the probability $[P(t) = 0.05 \sin(60\pi t)]$ of release of all presynaptic terminals j ($j = 1, 2, \ldots, 15$), at the most negative value of the sinusoid (valley), $p = 0$ and $p = 0.0025$ at the sinusoid peak. Each terminal had a absolute refractory time of 1 ms and a relative refractory time $[P_j(t) = R_j(t)P(t)]$ that obeyed a exponential function of the following form: $R_j(t) = e^{-0.1(t-t_{syn})}$. Synaptic parameters were chosen arbitrarily to produce a firing rate similar to the rate observed in kainate-induced gamma oscillations. In the study by Tiesinga et al. (2001) as well as in this work, the pyramidal cell model did not include the axon initial segment, the zone where APs are likely to be initiated (Kole et al., 2008). Data on the currents present on the initial segment are too sparse for the construction of a realistic axon initial segment compartment, and the scope of this paper was to assess the role of perisomatic I_M on the pyramidal cell function during gamma oscillations.

Results

M-current block decreases the power of kainate-induced gamma oscillations

Gamma oscillations in 400 μm hippocampal slices were induced by bath application of 100 nM kainate in a submerged recording chamber at 28°C. Slices that produced peak-to-peak oscillations smaller than 200 μV (in our experiments, ~30%) were discarded. It is possible that further optimized recording chambers would augment our success rate (Hájos et al., 2009) but oscillation amplitudes likely would not differ considerably from the amplitudes reported here (Hájos et al., 2009). Once induced and stabilized (~15 min after kainate perfusion), gamma oscillations lasted >1 h without any noticeable change in amplitude if perfusion rate and oxygenation were maintained (longer durations were not tested). To assess the effect of I_M block on gamma oscillations we bath applied 10 μM XE991, which caused a reduction of 32% in oscillation power (from 95 ± 32 to 56 ± 15 μV^2, $n = 20$, $p = 0.03$) without affecting the peak frequency (Fig. 1). In a second set of experiments, 20 μM bath-applied XE991 caused a reduction of 42% in oscillation power (from 86.7 ± 4.5 to 50.6 ± 5.4 μV^2, $n = 10$, $p < 0.01$), with no change in peak frequency or increase of power in low-frequency bands (Fig. 1). The higher concentration of 20 μM XE991 also reduced the power of gamma oscillations when slices were recorded at 35°C (39%, from 171.9 ± 41.95 to 104.4 ± 28.84 μV^2, $n = 6$, $p = 0.04$) (Fig. 1). In agreement with a previous study (Fisahn et al., 2002), the addition of 10 μM linopirdine did not affect either the power or the frequency of gamma oscillations (106.2 ± 13.2 to 108.6 ± 11.3 μV^2, $n = 4$) (supplemental Fig. 1, available at www.jneurosci.org as supplemental material). However, addition of either 20 or 40 μM linopirdine caused a significant reduction (29 or 30%, respectively) in gamma oscillation power (to 75.7 ± 7 or 74.3 ± 4.6 μV^2, respectively, $n = 4$, $p < 0.01$) (supplemental Fig. 1, available at www.jneurosci.org as supplemental material). We also observed a 23% decrease in gamma oscillation power when

10 μM linopirdine application was supplemented with 5 μM XE991 (from 102.76 ± 16.41 to 77.38 ± 7.51 μV^2, $n = 4$, $p = 0.03$, data not shown).

M-current block changes the firing pattern of CA3 pyramidal neurons during gamma oscillations

Next, we investigated the effect of XE991 on the firing pattern of CA3 pyramidal neurons during kainate-induced gamma oscillations (Fig. 2*A*). Once oscillations were established and showed constant amplitude for 5 min, we recorded 2 min of concomitant field and current-clamp data (control). After 15 min of application of 20 μM XE991 another 2 min of concomitant field and current-clamp data was recorded. Single gamma cycles were detected off-line using a sliding template function (Clements and Bekkers, 1997) and AP times were calculated in a time window equivalent to each gamma cycle (Fig. 2*B*). The mean membrane potentials (in the absence of APs, during interspike intervals) in the presence of 100 nM kainate were −56 ± 1.3 and −51.6 ± 0.6 mV when 20 μM XE991 was also present ($n = 8$, $p < 0.01$) (Fig. 2*C*,*D*). XE991 increased the firing rate of CA3 pyramidal neurons during gamma oscillations (Fig. 2*B–D*). Neurons fired APs in 6.2 ± 0.9% of the detected cycles before the addition of 20 μM XE991 and in 7.1 ± 1.2% after ($n = 8$, $p < 0.05$) (Fig. 2*C*,*D*). We have fitted normalized AP-firing histograms with a third-order polynomial of the form $ax^3 + bx^2 + cx$ (Eq. 1) to quantify the phase response of CA3 pyramidal neurons during a gamma cycle (Fig. 2*B*). If neurons fire more randomly, AP histograms would be expected to flatten and the value of *a* would move closer to zero. Average *a* value was 0.0086 ± 0.0011 before and 0.0036 ± 0.001 after the addition of 20 μM XE991 ($n = 8$, $p < 0.01$) (Fig. 2*B*,*D*). Average gamma cycles were aligned with AP-firing histograms to calculate the "preferred" firing phase angle of CA3 pyramidal neurons (angles >90° indicate that the peak firing occurred after the positive peak of the field oscillation) (Fig. 2*B–D*). The mean preferred firing phase angle was 117.8 ± 6.8° before and 26.8 ± 24.9° after 20 μM XE991 application ($n = 8$, $p < 0.01$) (Fig. 2*B*,*D*). In addition, application of 20 μM XE991 resulted in a greater variance of the peak firing angle compared with kainate-only control. The SD of the peak firing angle in control conditions was 19.1 but increased to 70.5 when XE991 was present ($p < 0.01$, *F* test) (Fig. 2*D*). We obtained similar results using field recordings concomitantly with cell-attached recordings. In cell-attached configuration, pyramidal cells fired APs in 6.7 ± 1.1% of the cycles (supplemental Fig. 2, available at www.jneurosci.org as supplemental material) in control and 12.13 ± 2.9% of the gamma cycles in the presence of 20 μM XE991 ($n = 4$, $p < 0.03$, paired *t* test) (supplemental Fig. 2, available at www.jneurosci.org as supplemental material). The preferred firing angle was equal to 133.4 ± 11.9° in control and 2.48 ± 45.14° in the presence of 20 μM XE991 ($n = 4$, $p < 0.03$, paired *t* test) (supplemental Fig. 2*B*,*D*, available at www.jneurosci.org as supplemental material) and *a* was equal to 0.18 ± 0.03 and 0.06 ± 0.01 for control and 20 μM XE991 ($n = 4$, $p < 0.05$, paired *t* test) (supplemental Fig. 2*B*,*D*, available at www.jneurosci.org as supplemental material).

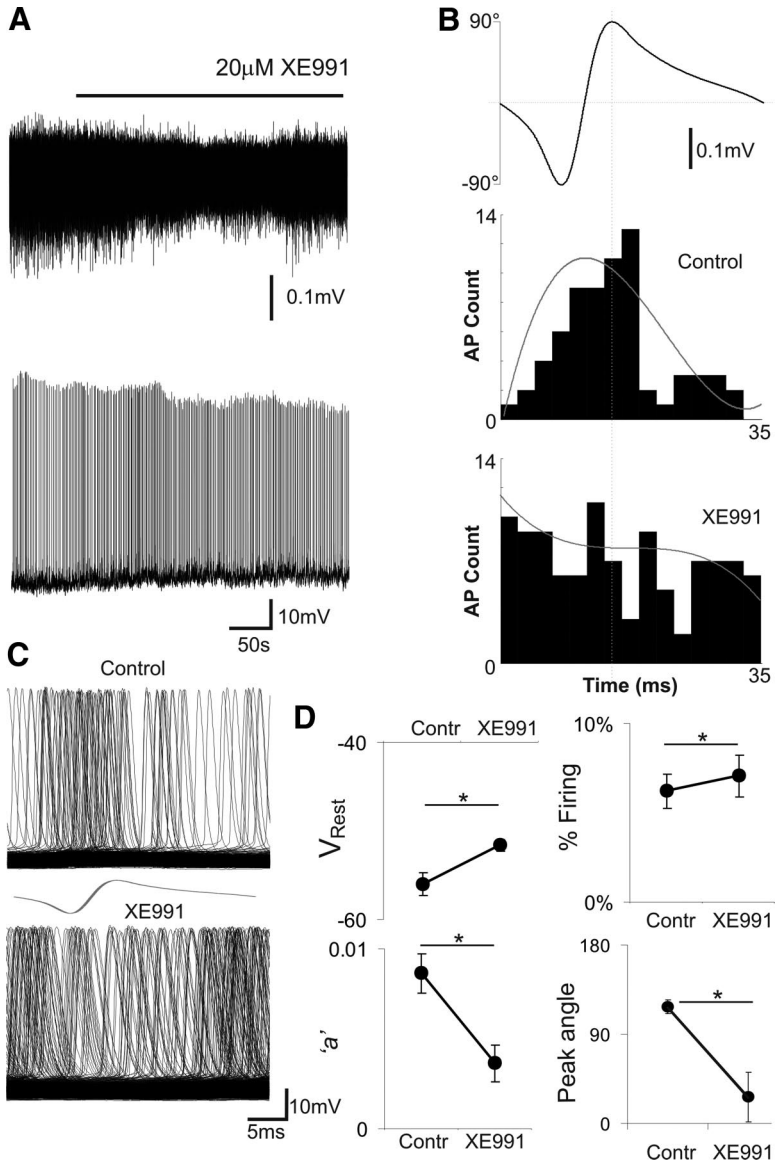

Figure 2. XE991 desynchronizes firing times of CA3 pyramidal neurons during gamma oscillations. ***A***, Example of concomitant field and current-clamp recordings from pyramidal neurons showing the decrease of oscillation power associated with the increase of CA3 pyramidal neuron firing frequency after the application of 20 μM XE991. ***B***, Average gamma cycle (top) and AP time histograms before (middle) and after (bottom) the addition of 20 μM XE991. AP time histograms were fitted with a third-order polynomial (gray traces) to quantify the "randomness" of AP times in relation to the gamma cycle (flatter histograms generate fits with smaller third-order coefficients). A 90° angle (vertical dashed line) was assigned to the peak of the oscillation cycle and the angle of the valley was equal to −90°. The arcsin (added by 90 or −90° if the AP-firing time occurred after the peak or the valley, respectively) of the normalized field oscillation was used to calculate the preferred firing angle. ***C***, Raw voltage traces of a pyramidal neuron in the presence of kainate showing differential AP alignment to the gamma cycle shown in ***B*** before and after the addition of XE991 (the layout of the average gamma cycle is also shown in gray between the voltage traces). ***D***, Summary of changes in basal membrane potential, percentage of gamma cycles in which APs were detected, third-order polynomial coefficient *a* (see Results), and position of AP time histogram peak in relation to the gamma cycle angle. Contr., Control. *$p < 0.03$.

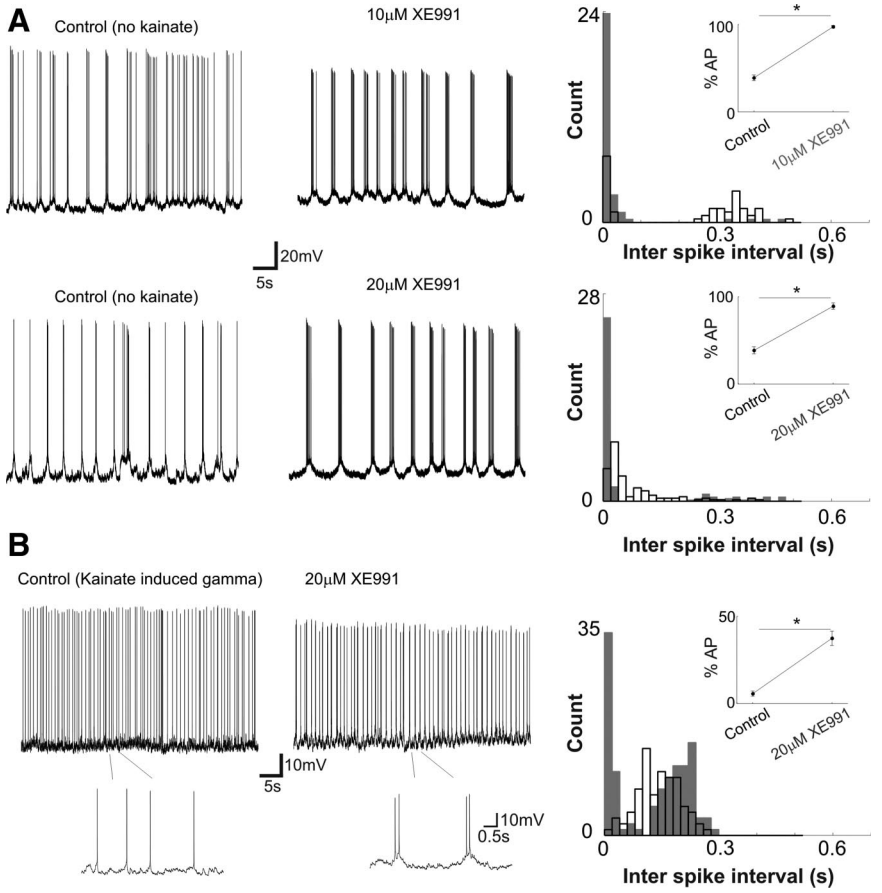

Figure 3. XE991 increases burst firing of CA3 pyramidal neurons. ***A***, Example of gap-free recordings of CA3 pyramidal neurons in the absence of kainate and presence of different concentrations of XE991. Histograms on the left show the interspike interval in control conditions (white bars) and in the presence of 10 μM XE991 (gray, top) and 20 μM XE991 (gray, bottom). Insets show the percentage of spikes that occurred <20 ms apart from each other. ***B***, Same as in ***A*** but during kainate-induced gamma oscillations. In these experiments only 20 μM XE991 was used. *$p < 0.02$.

XE991 increases burst firing in pyramidal neurons

During gap-free current-clamp recordings in the absence of kainate, pyramidal neurons can fire AP bursts (quantified by the percentage of APs that occur <20 ms from each other). Application of 10 μM XE991 increased the percentage of APs occurring <20 ms apart from 39 ± 4% of the total AP count to 89 ± 4% ($n = 4$, $p < 0.01$) (Fig. 3*A*). If 20 μM XE991 was applied to the bath, the percentage of closely spaced APs increased from 39 ± 3% to 97 ± 3% ($n = 4$, $p < 0.01$) (Fig. 3*A*). To avoid rundown of I_M due to prolonged recordings we tested the effect of 10 or 20 μM XE991 in different neurons instead of applying both concentrations in succession to the same neuron. In contrast to what is seen for theta oscillations (4–12 Hz) (Williams and Kauer, 1997), during gamma oscillations, pyramidal neurons do not fire in bursts (Fisahn et al., 1998). Our data confirm that after induction of gamma oscillations by kainate the percentage of APs fired in bursts (i.e., <20 ms apart) decreased from 39 ± 4% to 6 ± 1%. Subsequent application of 20 μM XE991 caused an increase in the percentage of APs fired <20 ms apart from 6 ± 1% to 37 ± 4% ($n = 8$, $p < 0.01$) (Fig. 3*B*).

XE991 and linopirdine differentially affect I_M

The effect of the I_M blocker XE991 and linopirdine on outward currents in voltage-clamp recordings of CA3 pyramidal neurons was further investigated. We first tested if we could record I_M in whole-cell configuration without rundown of the current by measuring the ratio between the instantaneous and steady-state outward current in response to a 0 mV voltage step in 5 min intervals. Prolonged whole-cell recordings caused a significant rundown of I_M. After 1 h of whole-cell recording, there was a decrease of 22.47% of the ratio between the steady-state and instantaneous outward current (see below) (0.27 ± 0.06 to 0.21 ± 0.04, $p = 0.04$, $n = 4$, paired t test) but no significant decrease was observed until 30 min from the establishment of whole-cell configuration (data not shown). We tried to minimize the effect of inward currents by perfusing the slices with 1 μM TTX, 50 μM $CdCl_2$, 20 μM ZD7288. Despite the usage of these blockers, we observed a substantial variability in the shape of outward currents recorded from CA3 pyramidal neurons (Fig. 4*A*). One-second-long voltage steps varying from −90 to 0 mV were applied after a −100 mV/1-s-long pre test step. XE991-sensitive currents were obtained by digitally subtracting the outward current before and 20 min after the addition of XE991. We recorded current responses to voltages up to 0 mV as the preparation generally became unstable after the application of more depolarizing voltage steps in the presence of XE991. At 0 mV there was a decrease of the total steady-state current by 40.8 ± 2.3% (measured at 990 ms from the test step onset) after the application of 10 μM XE991 (from 2.68 ± 0.5 nA to 1.44 ± 0.3 nA, $p < 0.03$, $n = 6$). A concentration of 20 μM XE991 caused a reduction of the steady-state current by 46 ± 5.3% (from 2.31 ± 0.12 nA to 1.25 ± 0.16 nA, $p < 0.02$, $n = 5$) and 10 μM linopirdine reduced the current by 36.1 ± 5.7% (from 2.53 ± 0.48 nA to 1.84 ± 0.49 nA, $p < 0.03$, $n = 5$) (Fig. 4*A*,*B*). There were no significant differences between the percentages of block (at 0 mV) after the application of 10 or 20 μM XE991 or 10 μM linopirdine. However, at −40 mV, the current sensitive to 10 μM linopirdine (after digital subtraction of the traces before and after linopirdine addition) represented only 6.4 ± 0.1% of the total linopirdine-sensitive current recorded at 0 mV, whereas these percentages were equal to 14.6 ± 3.3% and 23.5 ± 2.5% of the 10 and 20 μM XE991-sensitive currents, respectively (Fig. 4*B*).

Using our voltage-clamp recordings (20 μM XE991-sensitive currents) (Fig. 4*C*), we constructed an M-current model. The average time constants-versus-voltage and conductance-versus-voltage relationships are shown in Figure 4*D*. Least-mean square fit (using Eqs. 2 and 3, respectively) of these two relationships yields the following values: SF = 4135.76, Ca = 164.64 ms^{-1}, Cb = 0.33 ms^{-1}, $V_a = 0.118$ mV, $V_b = 0.097$ mV, $M = 35.66$ ms, $V_c = -0.0497$ mV, $V_{1/2} = 39.1465$ mV, and $k = 10.7530$ mV. Immunohistochemistry data suggest that the main source of I_M is located at the axon initial segment (Devaux et al., 2004). However, we were able to reasonably clamp the perisomatic I_M using somatic electrodes. Space-clamp errors in non-inactivating K^+ current recordings appear as small inactivation of the current and a nonsaturating g/V relationship (Bar-Yehuda and Korngreen,

2008) but our recordings clearly demonstrate a non-inactivating XE991-sensitive current (Fig. 4*C*) and a strong trend to saturation in the *g*/*V* relationship for the XE991-sensitive current (Fig. 4*D*).

We also tested the direct effect of 100 nM kainate and 20 μM muscarine on the I_M. Both these compounds can induce gamma-frequency field oscillations in hippocampal slices. The relative effect on I_M was estimated by the ratio between the time-dependent current (steady-state minus instantaneous current) and steady-state current (the minimum value of current after the onset of the current step) of current traces recorded in the presence of 1 μM TTX, 50 μM $CdCl_2$, 20 μM ZD7288 with or without 100 nM kainate or 20 μM muscarine. The time-dependent/steady-state current ratio was equal to 0.25 ± 0.03 before and 0.24 ± 0.05 after the application of 100 nM kainate (not significant, $n = 4$) (supplemental Fig. 3, available at www.jneurosci.org as supplemental material). In the presence of 20 μM muscarine, we observed a significant decrease in the time-dependent/steady-state current ratio (from 0.26 ± 0.06 to 0.15 ± 0.04, $p < 0.01$, $n = 4$) (supplemental Fig. 3, available at www.jneurosci.org as supplemental material).

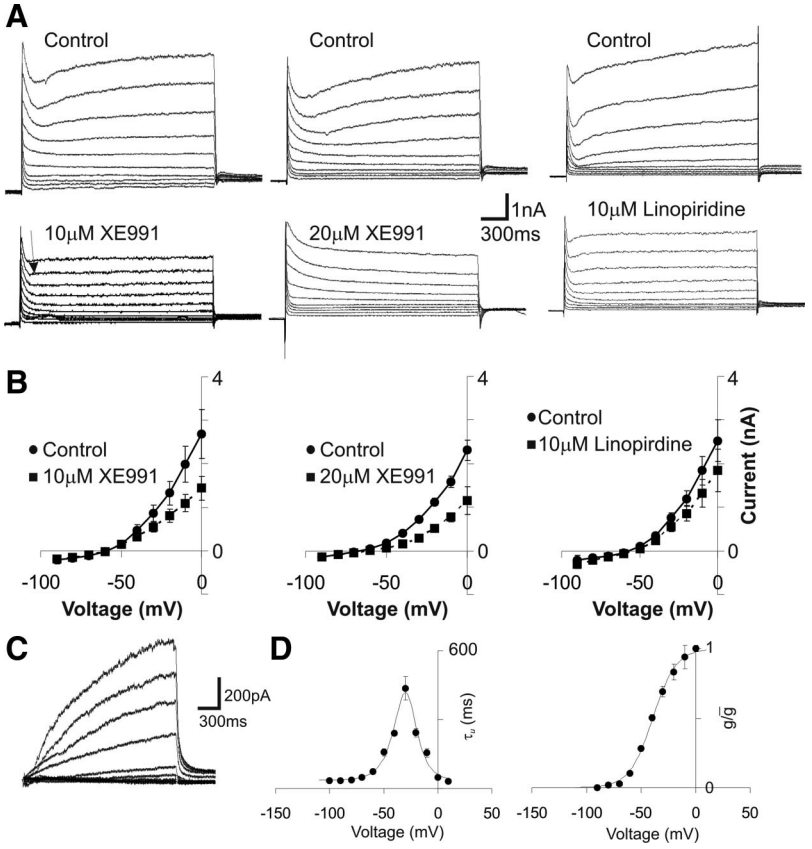

Figure 4. Linopirdine (10 μM) is insufficient to block M-currents at subthreshold potentials. ***A***, Example of a current response of a CA3 pyramidal neuron to voltage steps ranging from −90 to 0 mV in control conditions (top; in the presence of 1 μM TTX, 50 μM $CdCl_2$, and 20 μM ZD7288) and in the presence of 10 or 20 μM XE991 or 10 μM linopirdine (bottom). ***B***, Current–voltage relationships of outward currents (measured 50 ms before the end of the voltage test step) in control conditions and after the addition of 10 or 20 μM XE991 or 10 μM linopirdine. ***C***, Digitally subtracted current trace showing an example of the 20 μM XE991-sensitive component of the outward current of a CA3 pyramidal neuron. ***D***, Left, Summary of activation time constant-versus-voltage relationship (solid line shows the fit with Eq. 2). Note that the time constant value at 10 mV was added to improve the fit. Right, Normalized conductance of 20 μM XE991-sensitive currents-versus-voltage relationship (solid line shows the fitting with a Boltzmann function: Equation 3).

XE991 increases the excitability of pyramidal neurons

Current-clamp recordings in the absence of kainate showed that the addition of XE991 can cause a depolarization of membrane potential (V_{rest}), a decrease in the fast AHP and an increase in the number of APs fired in response to depolarizing current steps. In control conditions, the V_{rest} of CA3 pyramidal neurons was −62.4 ± 0.7 mV and the application of 10 μM XE991 depolarized the V_{rest} to −57.0 ± 1.2 mV ($n = 4$, $p < 0.01$) (Fig. 5). In control, AHP amplitude (the difference to the potential at the onset of the AP) was 2.9 ± 0.5 mV and decreased to 2.1 ± 0.28 mV after the application of 10 μM XE991 ($n = 4$, $p = 0.02$) (Fig. 5). Pyramidal neurons fired 1.5 ± 0.5 APs in control conditions in response to a 200-ms-long 100 pA current step and 1.75 ± 0.5 APs after the application of 10 μM XE991 ($n = 4$, not significant) (Fig. 5). The application of 20 μM XE991 caused a depolarization of V_{rest} from −62.5 ± 0.3 to −55 ± 0.7 mV, a decrease in AHP amplitude from 3.4 ± 0.3 to 1.8 ± 0.24 mV, and an increase of AP firing (in response to a 200-ms-long 100 pA current step) from 1.4 ± 0.22 to 3.1 ± 0.3 APs ($n = 10$, $p < 0.02$ for all cases) (Fig. 5).

I_M is important for the control of the transfer function of pyramidal neurons

Currents active around threshold are important determinants of the bandpass filtering and input/output gain control performed by pyramidal neurons (Cook et al., 2007) and, consequently, these currents can modulate subcellular oscillatory activity that, in turn, will modulate field oscillations. The role of the M-current as a modulator of resonant frequency (bandpass filtering) in the theta range (4–12 Hz) in pyramidal neurons has been shown in other studies (Hu et al., 2002; Peters et al., 2005). However, pyramidal neurons receive excitatory and inhibitory currents at frequencies much higher than the theta range during gamma oscillations (Fisahn et al., 1998). Additionally, Piccinin and colleagues (2006) have shown that I_M is essential for nonsynaptic gamma oscillations in the hippocampus. Thus, the filtering properties of pyramidal neurons for inputs at frequencies around the gamma range may also be important in determining firing properties of pyramidal neurons. To analyze the filtering properties of the cell membrane and the role of I_M in determining these properties, we have applied a chirp signal (120 pA peak to peak) with a linear increase of frequency from 5 to 40 Hz over 10 s in current clamp (in the presence of 1 μM TTX). The normalized transfer function (the relation between the input current and output voltage) in the frequency domain was 3.5 ± 0.3 (at 30 Hz) in control conditions and 3 ± 0.5 after the addition of 10 μM XE991 ($n = 4$, not significant) (Fig. 6). However, if 20 μM XE991 was applied to the bath, the normalized transfer function amplitude decreased from 3.3 ± 0.2 to 2.1 ± 0.3 ($n = 4$, $p < 0.03$) (Fig. 6). Hence, the addition of 20 μM XE991 augments the filtering of subthreshold inputs at frequencies in the gamma range.

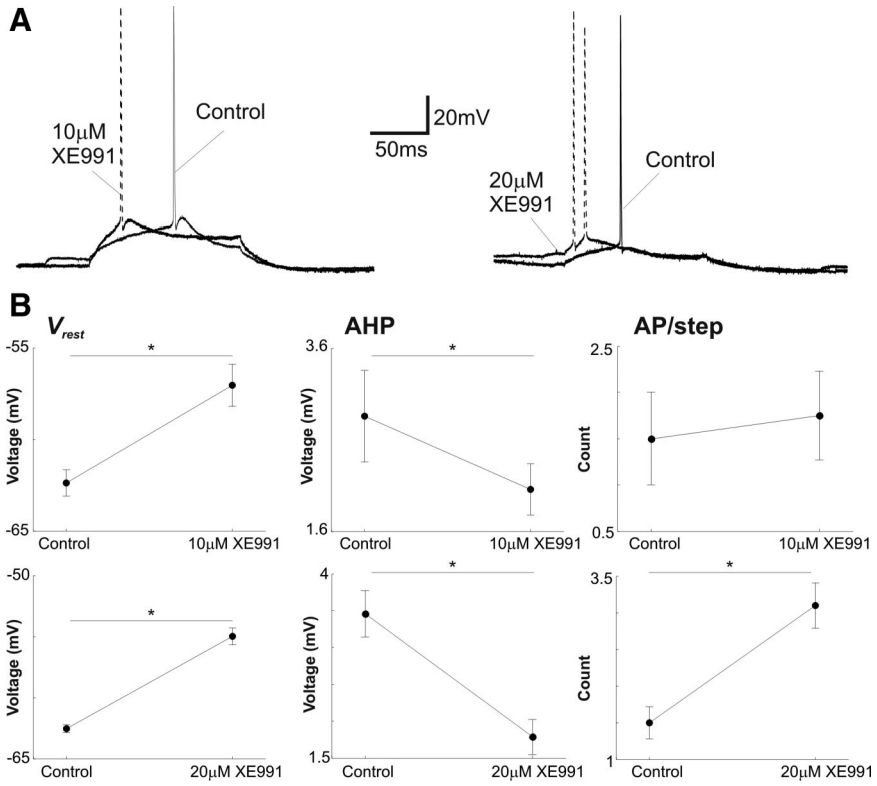

Figure 5. Firing properties of CA3 pyramidal neurons are altered by M-current block. ***A***, Examples of voltage responses of CA3 pyramidal neurons to 100 pA current steps in control (solid traces) and in the presence of external 10 μM XE991 (dashed trace, left) and 20 μM XE991 (dashed trace, right). ***B***, Summary of resting membrane potential (V_{rest}), AHP voltage, and number of APs in a 200-ms-long 100 pA current step in control and external 10 μM XE991 (top) or 20 μM XE991 (bottom). *$p < 0.01$.

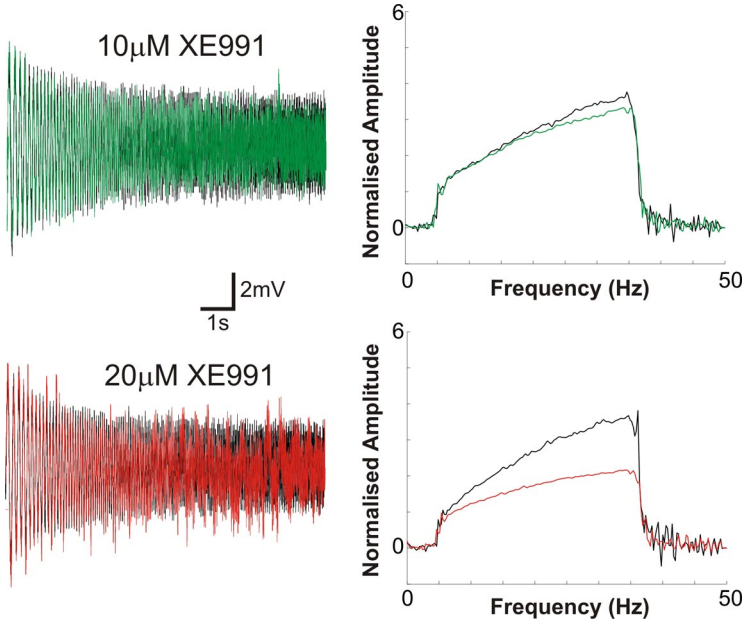

Figure 6. Blocking I_M augments the low-pass filtering of injected currents in CA3 pyramidal neurons. Left, Examples of the voltage response of a pyramidal neuron to the injection of a 10-s-long chirp current waveform (frequency changing linearly from 5 to 40 Hz) in control conditions (black traces) and in the presence of 10 μM XE991 (green trace, top) or 20 μM XE991 (red trace, bottom). The membrane potentials of these two cells were equal to −61.6 mV (control, top black trace), −62.1 mV (control, bottom trace), and −58.4 mV (top green trace) after the addition of 10 μM XE991 and −56.1 mV (bottom red trace) after the addition of 20 μM XE991. Right, Examples of transfer function estimates (input/output relationship in the frequency domain) in control conditions (black traces) and in the presence of 10 μM XE991 (green trace, top) or 20 μM XE991 (red trace, bottom). Both current and voltage were normalized before estimation of the transfer function.

Addition of a simulated M-current improves phasic firing of pyramidal neurons

To further elucidate the role of pyramidal neuron I_M in shaping neuronal firing during gamma oscillations we have used dynamic clamp to simulate I_M in neurons in which the native current was suppressed. Using an internal recording solution containing 0.5 mM $BaCl_2$ we blocked the native I_M of single pyramidal neurons (Lamas et al., 1997). At this concentration the barium salt did not significantly affect the hyperpolarization-activated current (data not shown). $BaCl_2$ can also block a variety of other K^+ channels (e.g., inward rectifier, leak channels, etc.) (Coetzee et al., 1999). In the presence of kainate, pyramidal neurons are depolarized to potentials considerably above the range in which inward rectifier channels are active. Regarding the $BaCl_2$ effect on leak channels, we did not observe a significant difference between input resistance between recordings in the presence of 20 μM XE991 and experiments performed with $BaCl_2$ in the internal recording solution (data not shown). Outward currents recorded in the presence of TTX and ZD7288 were similar to outward currents observed when 20 μM XE991 was present in the bath (Figs. 4*A*, 7*A*). To demonstrate this similarity, we measured the ratio between the time-dependent current and steady-state current of current traces recorded in the presence of 20 μM XE991 in the bath and compared it to the same ratio when the internal recording solution was supplemented with $BaCl_2$ instead of XE911 application. At 0 mV, these current ratios were 0.25 ± 0.05 (control), 0.05 ± 0.02 (XE991 bath application), and 0.07 ± 0.02 (intracellular $BaCl_2$ application; $n = 8$) (Fig. 7*B*). While there was a significant difference between the control group (neither XE991 nor $BaCl_2$) and both the external 20 μM XE991 and internal $BaCl_2$ groups ($p < 0.01$ and $p < 0.05$, respectively), no significant differences were observed in the current ratios between the recordings performed with 20 μM XE991 added to the bath and with an internal recording solution supplemented with $BaCl_2$ (Fig. 7*B*).

By blocking the native I_M of single neurons, we could test whether postsynaptic I_M contributes to the firing pattern of pyramidal neurons during gamma oscillations. By subsequently reintroducing I_M using the dynamic clamp technique, we could test whether this current could rescue the native firing phenotype of CA3 pyramidal neurons. The ability of

our simulated I_M to emulate the native I_M was tested by applying current steps (−300 to 300 pA in 50 pA increments, 200 ms long) in normal ACSF using 0.5 mM $BaCl_2$ in the internal solution (for reasons see Materials and Methods page 5) with or without the simulated I_M (dynamic clamp, $\bar{g}_M$ = 13 nS). When our internal solution contained 0.5 mM $BaCl_2$, V_{rest} was −55.2 ± 2 mV without and −62.1 ± 1 mV with the I_M dynamic clamp (n = 7, $p < 0.01$) (Fig. 7*C*,*D*). In the same conditions, AHP amplitude was 2.29 ± 0.2 mV without and 1.29 ± 0.2 mV with the I_M dynamic clamp (n = 7, $p < 0.01$) (Fig. 7*C*,*D*). In addition, when the internal recording solution contained 0.5 mM $BaCl_2$, pyramidal neurons responded with 2.3 ± 0.2 APs but the same neurons fired 1.3 ± 0.2 APs if the simulated I_M was applied to the cell (n = 7, $p < 0.01$) (Fig. 7*C*,*D*).

During kainate-induced gamma oscillations CA3 pyramidal neurons that had $BaCl_2$ dialyzed into their cytoplasm showed an atypical firing pattern in relation to the field oscillation cycle. Without the I_M dynamic clamp, cells fired APs in 8.8 ± 0.9% of the cycles, whereas with the dynamic clamp (g_M = 13 nS), APs were fired only in 4.8 ± 0.6% of the cycles (n = 6, $p < 0.01$) (Fig. 8*A*,*C*). The potential was −52.4 ± 1.15 mV in the absence and −56.4 ± 1.23 mV in the presence of I_M dynamic clamp (n = 6, $p < 0.01$) (Fig. 8*A*,*C*). The third-order coefficient a (calculated by fitting the normalized AP time histogram with Eq. 1) was 0.01 ± 0.003 before and 0.03 ± 0.008 after the addition of the simulated I_M ($n = 6, p < 0.02$) (Fig. 8*B*,*C*). Mean preferred firing angle was 39.3 ± 47° before and 98.2 ± 2.8° after the I_M dynamic clamp ($n = 6, p < 0.01$) (Fig. 8*B*,*C*). SDs were also significantly larger for preferred firing phase angle before (282.2) compared with after (17) the addition of the I_M dynamic clamp ($n = 6, p < 0.01$) (Fig. 8*C*).

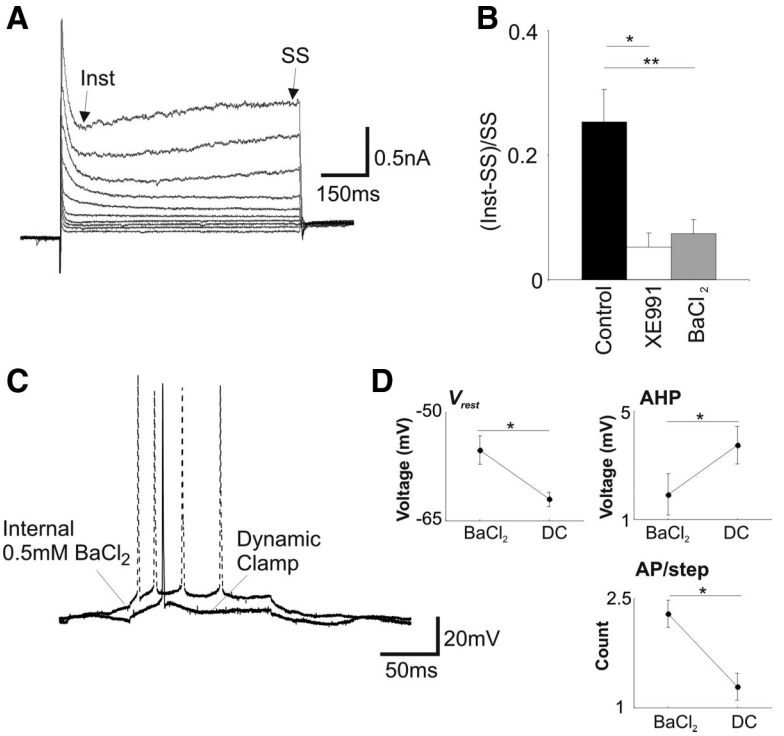

Figure 7. Altered firing properties due to M-current block in the absence of kainate can be rescued by an I_M dynamic clamp. ***A***, Example of a voltage-clamp recording (same protocol as in Fig. 2) showing the effect of 0.5 mM $BaCl_2$ in the internal recording solution on the M-current. Arrows indicate the regions where the instantaneous (Inst) and steady-state (SS) currents were measured. ***B***, Summary of (SS − Inst)/SS ratios of outward currents (in response to a 0 mV voltage step) in control conditions, after the addition of 20 μM XE991, and when 0.5 mM $BaCl_2$ was present in the internal solution. ***C***, Example of a current-clamp recording (200 ms, 100 pA current step) of a pyramidal neuron using an internal solution supplemented with 0.5 mM $BaCl_2$ with (solid trace) and without (dashed trace) the simulated I_M (dynamic clamp). ***D***, Summary of V_{rest}, AHP voltage, and numbers of APs in response to a 100 pA current step recorded with internal $BaCl_2$ before and after the DC. *$p < 0.03$.

The role of I_M in determining pyramidal neuron firing in response to noisy (or sparsely synchronized) inputs was further evaluated using a simplified CA3 pyramidal neuron model. IPSP and EPSP times were determined by a 30 Hz sinusoid. Because our model used a low synaptic probability, the neuron fired APs with no evident rhythm (Fig. 9). When $\bar{g}_M$ equaled 13 nS, the modeled neuron fired APs in 4% of the cycles, whereas when $\bar{g}_M$ equaled 0 nS, APs were fired in 11% of the cycles (Fig. 9). The peaks of the AP time histogram coincided with an oscillation phase of −12 and 102° if $\bar{g}_M$ equaled 13 nS and 36 and 102° when $\bar{g}_M$ equaled 0 (Fig. 9*B*). We simulated the effect of a voltage-dependent block of I_M by linopirdine by multiplying Equation 4 with a voltage-dependent scaling function $\gamma(V)$ as follows:

$$\gamma(V) = 1 - 0.76/(1 + e^{-(V+51.4061)0.2149}). \quad (7)$$

The function $\gamma(V)$ is based in the work of Romero et al. (2004). Multiplying Equation 4 with $\gamma(V)$ results in a reduction of only 10% of I_M at −60 mV and 76% at 0 mV. When I_M was affected by a voltage-dependent blocker, the simulated neuron fired in 5% of the cycles and the peak of AP time histogram coincided with an oscillation angle of 30° (Fig. 9*B*). We also tested the importance of the compartmentalization of I_M by moving I_M to the dendritic compartment. When I_M was present only in the dendrite the neuron fired APs in 9% of the oscillation cycles and the peak of the AP time histogram coincided with an oscillation angle of 54° (Fig. 9*B*). Third-order coefficients of the polynomial fit of AP time histogram were a = 0.18 for the model with a somatic $\bar{g}_M$ = 13 nS, a = 0.05 for the model with a somatic $\bar{g}_M$ = 0 nS, and a = 0.14 for the model with a somatic $\bar{g}_M$ = 13 nS but with the voltage-dependent block implemented. The third-order coefficient of the polynomial fit was a = 0.06 when I_M was placed in the dendrite instead of the soma. Another aspect explored in our simulations was the effect of eliminating I_M when the cell received tonic excitation and rhythmical inhibition (Traub et al., 2000; Hájos et al., 2004). Tonic excitation was provided by the injection of 100 pA current at the soma of the modeled cell, whereas inhibitory synaptic inputs were as described in Materials and Methods. When I_M was intact ($\bar{g}_M$ = 13 nS), the modeled neuron fired APs in 11% of the cycles, the peak of the AP time histogram coincided with an oscillation angle of −114°, and the third-order coefficient of the polynomial fit was a = 0.11. For $\bar{g}_M$ = 0 nS, those values were equal to 28%, −90 and 138° (two equal AP time histogram peaks), and a = 0.04, respectively (Fig. 9*C*). The model data suggest that a perisomatic I_M is more efficient in controlling the firing phase of the neuron in response to noisy but rhythmical inputs than a dendritic I_M and that, to unmask the effect of I_M, it is necessary to fully block KCNQ channels at voltages around the resting potential.

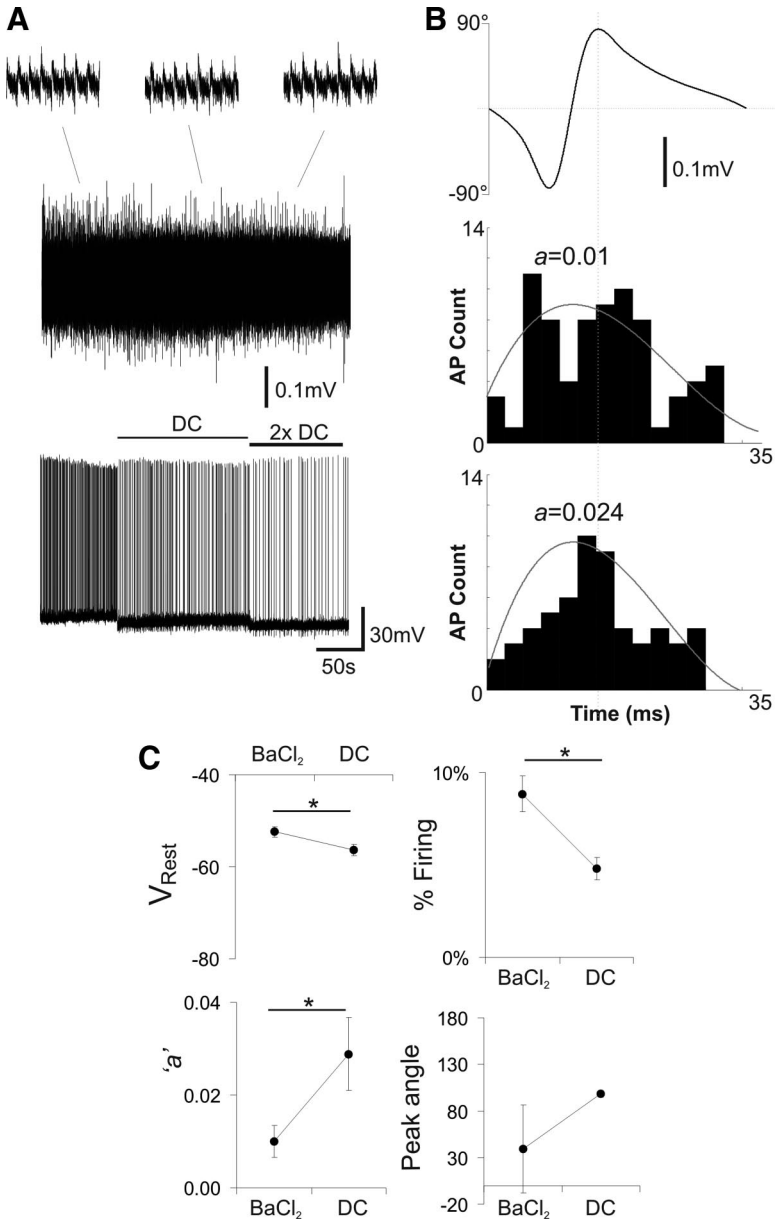

Figure 8. Addition of a modeled M-current to CA3 pyramidal neurons improves phase preference firing during gamma oscillations. ***A***, Example of a field recording and a simultaneous CA3 whole-cell current-clamp recording of a pyramidal neuron (0.5 mM $BaCl_2$ was added to the internal solution to block the native M-current). A simulated M-current was added to the neuron using the average M-current conductance g_M (DC) and $2\times$ g_M ($2\times$ DC). ***B***, Average gamma cycle (top) and AP time histograms with their respective third-order polynomial fits (gray traces) before (middle) and after (bottom) the addition of the modeled M-current. The vertical dashed line shows the position of the positive oscillation peak (90°). ***C***, Summary of changes in basal membrane potential, percentage of gamma cycles with APs, third-order polynomial coefficient, and position of AP time histogram peak in relation to the gamma cycle angle before and after the addition of the artificial M-current. *$p < 0.02$.

Discussion

In this study we have shown that I_M is an important modulator of the firing phase of CA3 pyramidal neurons during *in vitro* gamma oscillations in the hippocampus. We first demonstrated that application of XE991, an I_M blocker, decreases field oscillation amplitude. We next described a significant loss of synchrony between field activity and pyramidal cell firing in the presence of XE991. In addition, the decrease in synchrony observed when I_M was decremented in a single cell was reversed if a simulated I_M was applied to the cell via dynamic clamp. Whereas the results of a previous study suggested that I_M was not important for the maintenance of *in vitro* gamma oscillations (but rather I_h and I_{cat}) (Fisahn et al., 2002), this discrepancy can be explained by different induction protocols used (carbachol- vs kainate-induced gamma oscillations) and the higher potency of the M-current blocker used in this study. Carbachol/muscarine induction protocols involve the activation of metabotropic receptors that have well described effects on I_M (Brown and Adams, 1982), while the application of kainate activates mostly ionotropic kainate receptors, and we did not observe any direct effects on I_M. However, it is interesting to note how gamma oscillations induced by the activation of different receptor families appear to be similar macroscopically (Traub et al., 2002; Fisahn et al., 2004). Also, in the study by Fisahn et al. (2002), the authors applied 10 μM linopirdine to block I_M, and at this concentration linopirdine has a very small effect on M-currents at resting membrane potential as a later study by Romero et al. (2004) showed. The larger difference in the percentage of I_M block by these two compounds at -40 mV when compared with the percentage of block at 0 mV can be explained by the voltage-dependent effect of both XE991 and linopirdine (Romero et al., 2004). Due to the higher potency of XE991 we could observe a significant decrease of I_M at voltages close to V_{rest}. Hence, the 10 μM linopirdine used in the study by Fisahn et al. (2002) to examine the effect of I_M block on gamma oscillations was insufficient to affect I_M significantly at V_{rest}. Our pyramidal neuron model also shows that a voltage-dependent block of I_M does not change the pyramidal neuron transfer function as dramatically as a total block of that current.

Here we have used XE991, a compound $10\times$ more potent than linopirdine (Romero et al., 2004). XE991 affected V_{rest} and altered AHP size and bursting activity, whereas 10 μM linopirdine showed almost no effect on the resting potential of pyramidal neurons (data not shown). Ten micromoles XE991 caused a substantial reduction in gamma oscillations (by 32%) and double that concentration decreased the oscillation power even further (by 42%). Ten micromoles XE991 is $>10\times$ the IC_{50} for this compound when measured at a membrane potential of -30 mV (Romero et al., 2004) and one would expect this concentration to block the majority (if not all) KCNQ channels in hippocampal slices. In fact, both concentrations caused an increase in burst firing in the absence of current injection and a depolarization of V_{rest} (~5 and 7 mV, respectively). However, these effects were generally greater when 20 μM XE991 was applied to the bath, indicating the presence of an unblocked fraction of I_M at resting potentials if 10 μM XE991 was used. This fraction

might be responsible for the greater decrease in gamma oscillation power observed in the presence of 20 μM XE991. Small variations in V_{rest} can alter substantially the firing properties of pyramidal neurons during gamma oscillations (Fisahn et al., 2004); hence, the further block of KCNQ channels near resting potential caused by 20 μM XE991 could explain the larger effect we observed on pyramidal neuron firing.

Our voltage-clamp data suggest that at 20 μM, XE991 did not affect currents other than I_M. However, XE991 is not as specific as previously suggested. At greater concentrations (40 μM) XE991 causes a reduction in the fast inactivating K^+ current (I_A) (R. N. Leão and A. Fisahn, unpublished data). It is also known that concentrations of ~100 μM XE991 can block ERG channels (Elmedyb et al., 2007). Furthermore, it is important to note that there was a large variability in the kinetics of outward currents recorded from CA3 neurons (Fig. 4*A*). However, the kinetics of XE991-sensitive currents appear to be more homogeneous among different CA3 pyramidal neurons than other outward currents (Fig. 4*C*). To obtain a "clean" I_M from digital subtraction, we had to apply TTX and $CdCl_2$ to block fast inactivating Na^+ and Ca^{2+} (and Ca^{2+}-dependent) currents. Vanner and colleagues (1993) have shown that 200 μM $CdCl_2$ can partially block (~60%) M-like currents. We used 4× less $CdCl_2$ in this study and to our knowledge this concentration has little effect on I_M. Also, the kinetics of our XE991-sensitive currents are highly suggestive of a "pure" I_M.

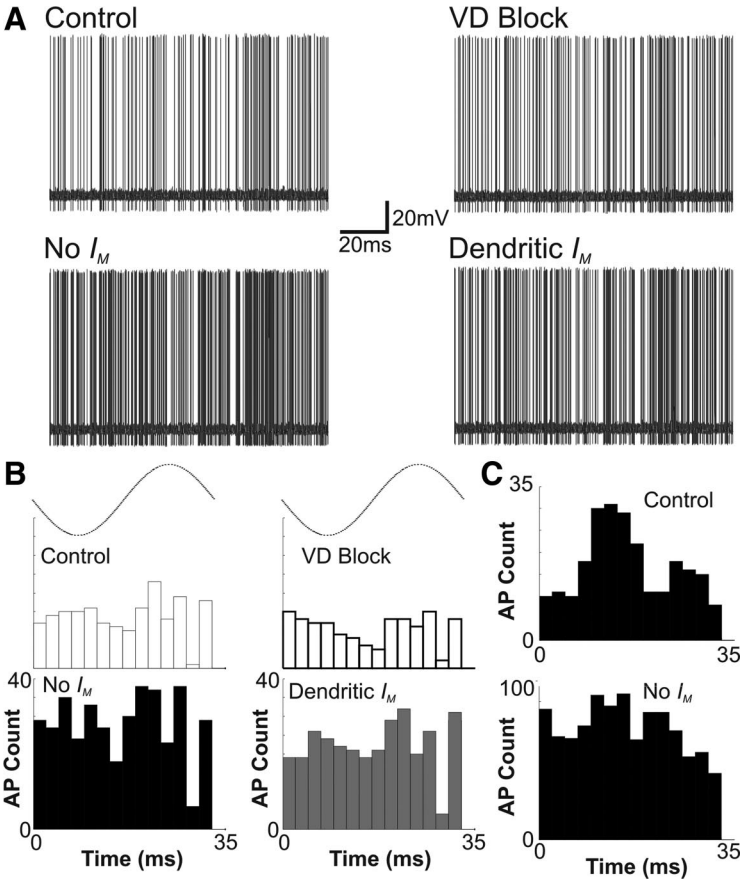

Figure 9. In a compartmental pyramidal neuron model I_M decreases firing rate and randomness of action potentials. ***A***, Model voltage response to rhythmic synaptic activity (see Materials and Methods) in control conditions ($g_M = 13$ nS; top left), when no I_M was implemented in the neuron ($g_M = 0$ nS; bottom left), when a voltage-dependent block was applied to M-channels (top right), and when M-channels were implemented in the dendrite rather than the soma (bottom right). ***B***, AP time histograms in relation to a gamma oscillation cycle (dotted lines) for the conditions shown in ***A***. ***C***, AP time histogram of a model cell that received rhythmical inhibition and tonic excitation when $g_M = 13$ nS (top) and 0 nS (bottom).

In hippocampal neurons, I_M is responsible for spike frequency adaptation (Storm, 1990), for the maintenance of the resting potential (Brown et al., 1990), for preventing burst firing (Vervaeke et al., 2006) and, together with I_h, for the generation of subcellular theta oscillations (Gu et al., 2005). Therefore, I_M can alter the input/output relationship of pyramidal neurons contributing to the sparse single firing displayed by these cells during *in vitro* gamma oscillations (Fisahn et al., 2004). Our experiments have shown that without I_M, low-pass filtering for gamma oscillation-frequencies is increased, indicating that I_M can modulate the way pyramidal neurons process subthreshold inputs. Also, there is an increase in burst firing after the addition of XE991 that could disrupt oscillations by altering the AP timing of pyramidal neurons.

Obviously, interneurons will be affected by XE991 also, and this effect conceivably could contribute to the decrease in gamma power we describe here (Fuchs et al., 2007). Lawrence and colleagues (2006) have shown that I_M is a major determinant of interspike interval of hippocampal interneurons and future experiments should address the effect of I_M block in different interneuron populations during gamma oscillations. The scope of this study was to demonstrate that I_M modulates pyramidal neuron firing and that this modulation can explain the decrease in gamma oscillations caused by XE991. To separate the subcellular and the network effects of I_M, we created an I_M model based on our voltage-clamp results and applied the modeled current to pyramidal neurons that had their native I_M blocked by intracellularly applied $BaCl_2$. Current-clamp recordings with Ba^{2+} in the intracellular solution have shown that the preferred firing angle of pyramidal neurons during gamma oscillations is quite different from cells recorded with intact I_M despite intact ongoing oscillations and synaptic input. A firing behavior similar to pyramidal neurons in control conditions was observed when we added artificial I_M to cells using dynamic clamp. Blocking I_M in a single cell did not produce the dramatic change in the AP time histogram observed when XE991 was applied globally. However, in the latter case, there is a global decrease in the field oscillation power while in the former experiments, the synaptic drive is intact. Using a simplified pyramidal neuron model, we have shown that I_M can alter the preferred firing phase angle of a pyramidal neuron and that a model without I_M displays a flatter AP time histogram in response to rhythmical inputs.

It is important to note that the subcellular localization of I_M dramatically affects the function of this current (Hu et al., 2007). Immunohistochemistry experiments have shown that KCNQ3 channels are mostly localized in the axons of CA3 pyramidal neurons (Devaux et al., 2004). Our dynamic clamp experiments were performed in somatic recordings, simulating only periso-

matic I_M. However $BaCl_2$ could have diffused to distal compartments, producing a distal block of I_M that could not be compensated for by the dynamic clamp technique. I_M channels responsible for controlling somatic excitability are located proximal to the soma region (Devaux et al., 2004; Hu et al., 2007). Also, by rescuing the normal response of CA3 neurons in field oscillations, our dynamic clamp experiments have demonstrated that I_M is essential for pyramidal neurons to maintain coherent firing during gamma oscillations. These experiments have also shown that I_M can modulate pyramidal neuron firing only by its voltage dependence. Additionally, using a two-compartment model we have demonstrated that perisomatic I_M is more efficient than dendritic I_M in decreasing AP frequency and phase locking the pyramidal neuron firing to synchronous inputs. It will be interesting in future experiments to reassess the cholinergic modulation of I_M during gamma oscillations.

In this work, we demonstrate that I_M, a current active around threshold, is an important modulator of neuronal excitability during oscillatory activity. While this study is devoted to the role of I_M in the computation of dendrosomatic inputs, the axonal location of KCNQ suggests that this current might also modulate axonal excitability (Devaux et al., 2004; Pan et al., 2006). KCNQ channels have motifs similar to Na^+ channel proteins that cause the retention of these channels in the axon (Pan et al., 2006) and the strategic placement of I_M in the initial segment could serve as a blocker of backpropagating action potentials and a decoupling between soma and axon. The axonal placement of I_M is particularly important for the analysis of *in vitro* oscillations as some studies have suggested that intrinsic axonal activity in pyramidal cells is essential to the generation of rhythmic activity (Traub et al., 2002, 2003). However, the role of axons and backpropagating action potentials in gamma oscillations still needs to be addressed experimentally before studying the importance of I_M in the axonal compartment. Nevertheless, we have shown that perisomatic I_M can modulate the transfer function of the somatodendritic compartment. The results shown here demonstrate that intrinsic neuronal properties are important determinants of network oscillations *in vitro* and that I_M has a significant impact on gamma oscillations, which, in turn, play a significant role in cognitive function.

References

Bar-Yehuda D, Korngreen A (2008) Space-clamp problems when voltage clamping neurons expressing voltage-gated conductances. J Neurophysiol 99:1127–1136.

Börjesson A, Karlsson T, Adolfsson R, Rönnlund M, Nilsson L (1999) Linopirdine (DUP 996): cholinergic treatment of older adults using successive and non-successive tests. Neuropsychobiology 40:78–85.

Brown DA, Adams PR (1980) Muscarinic suppression of a novel voltage-sensitive K+ current in a vertebrate neurone. Nature 283:673–676.

Brown DA, Gähwiler BH, Griffith WH, Halliwell JV (1990) Membrane currents in hippocampal neurons. Prog Brain Res 83:141–160.

Clements JD, Bekkers JM (1997) Detection of spontaneous synaptic events with an optimally scaled template. Biophys J 73:220–229.

Coetzee WA, Amarillo Y, Chiu J, Chow A, Lau D, McCormack T, Moreno H, Nadal MS, Ozaita A, Pountney D, Saganich M, Vega-Saenz de Miera E, Rudy B (1999) Molecular diversity of K+ channels. Ann N Y Acad Sci 868:233–285.

Cook EP, Wilhelm AC, Guest JA, Liang Y, Masse NY, Colbert CM (2007) The neuronal transfer function: contributions from voltage- and time-dependent mechanisms. Prog Brain Res 165:1–12.

Devaux JJ, Kleopa KA, Cooper EC, Scherer SS (2004) KCNQ2 is a nodal K+ channel. J Neurosci 24:1236–1244.

Dickinson R, Awaiz S, Whittington MA, Lieb WR, Franks NP (2003) The effects of general anaesthetics on carbachol-evoked gamma oscillations in the rat hippocampus in vitro. Neuropharmacology 44:864–872.

Elmedyb P, Calloe K, Schmitt N, Hansen RS, Grunnet M, Olesen SP (2007) Modulation of ERG channels by XE991. Basic Clin Pharmacol Toxicol 100:316–322.

Fisahn A (2005) Kainate receptors and rhythmic activity in neuronal networks: hippocampal gamma oscillations as a tool. J Physiol 562:65–72.

Fisahn A, Pike FG, Buhl EH, Paulsen O (1998) Cholinergic induction of network oscillations at 40 Hz in the hippocampus in vitro. Nature 394:186–189.

Fisahn A, Yamada M, Duttaroy A, Gan JW, Deng CX, McBain CJ, Wess J (2002) Muscarinic induction of hippocampal gamma oscillations requires coupling of the M1 receptor to two mixed cation currents. Neuron 33:615–624.

Fisahn A, Contractor A, Traub RD, Buhl EH, Heinemann SF, McBain CJ (2004) Distinct roles for the kainate receptor subunits GluR5 and GluR6 in kainate-induced hippocampal gamma oscillations. J Neurosci 24:9658–9668.

Fisahn A, Neddens J, Yan L, Buonanno A (2009) Neuregulin modulates hippocampal gamma oscillations: implications for schizophrenia. Cereb Cortex 19:612–618.

Fuchs EC, Zivkovic AR, Cunningham MO, Middleton S, Lebeau FE, Bannerman DM, Rozov A, Whittington MA, Traub RD, Rawlins JN, Monyer H (2007) Recruitment of parvalbumin-positive interneurons determines hippocampal function and associated behavior. Neuron 53:591–604.

Gu N, Vervaeke K, Hu H, Storm JF (2005) Kv7/KCNQ/M and HCN/h, but not KCa2/SK channels, contribute to the somatic medium after-hyperpolarization and excitability control in CA1 hippocampal pyramidal cells. J Physiol 566:689–715.

Hájos N, Pálhalmi J, Mann EO, Németh B, Paulsen O, Freund TF (2004) Spike timing of distinct types of GABAergic interneuron during hippocampal gamma oscillations *in vitro*. J Neurosci 24:9127–9137.

Hájos N, Ellender TJ, Zemankovics R, Mann EO, Exley R, Cragg SJ, Freund TF, Paulsen O (2009) Maintaining network activity in submerged hippocampal slices: importance of oxygen supply. Eur J Neurosci 29:319–327.

Halliwell JV, Adams PR (1982) Voltage-clamp analysis of muscarinic excitation in hippocampal neurons. Brain Res 250:71–92.

Hu H, Vervaeke K, Storm JF (2002) Two forms of electrical resonance at theta frequencies, generated by M-current, h-current and persistent Na+ current in rat hippocampal pyramidal cells. J Physiol 545:783–805.

Hu H, Vervaeke K, Storm JF (2007) M-channels (Kv7/KCNQ channels) that regulate synaptic integration, excitability, and spike pattern of CA1 pyramidal cells are located in the perisomatic region. J Neurosci 27:1853–1867.

Kole MH, Ilschner SU, Kampa BM, Williams SR, Ruben PC, Stuart GJ (2008) Action potential generation requires a high sodium channel density in the axon initial segment. Nat Neurosci 11:178–186.

Lamas JA, Selyanko AA, Brown DA (1997) Effects of a cognition-enhancer, linopirdine (DuP 996), on M-type potassium currents (IK(M)) and some other voltage- and ligand-gated membrane currents in rat sympathetic neurons. Eur J Neurosci 9:605–616.

Lawrence JJ, Saraga F, Churchill JF, Statland JM, Travis KE, Skinner FK, McBain CJ (2006) Somatodendritic Kv7/KCNQ/M channels control interspike interval in hippocampal interneurons. J Neurosci 26:12325–12338.

Leao RN, Svahn K, Berntson A, Walmsley B (2005) Hyperpolarization-activated (Ih) currents in auditory brainstem neurons of normal and congenitally deaf mice. Eur J Neurosci 22:147–157.

Mann EO, Paulsen O (2005) Mechanisms underlying gamma ('40 Hz') network oscillations in the hippocampus—a mini-review. Prog Biophys Mol Biol 87:67–76.

Mann EO, Suckling JM, Hajos N, Greenfield SA, Paulsen O (2005) Perisomatic feedback inhibition underlies cholinergically induced fast network oscillations in the rat hippocampus in vitro. Neuron 45:105–117.

Oren I, Mann EO, Paulsen O, Hájos N (2006) Synaptic currents in anatomically identified CA3 neurons during hippocampal gamma oscillations in vitro. J Neurosci 26:9923–9934.

Pan Z, Kao T, Horvath Z, Lemos J, Sul JY, Cranstoun SD, Bennett V, Scherer SS, Cooper EC (2006) A common ankyrin-G-based mechanism retains KCNQ and NaV channels at electrically active domains of the axon. J Neurosci 26:2599–2613.

Pedarzani P, Storm JF (1995) Protein kinase A-independent modulation of

ion channels in the brain by cyclic AMP. Proc Natl Acad Sci U S A 92:11716–11720.

Piccinin S, Randall AD, Brown JT (2006) KCNQ/Kv7 channel regulation of hippocampal gamma-frequency firing in the absence of synaptic transmission. J Neurophysiol 95:3105–3112.

Pinsky PF, Rinzel J (1994) Intrinsic and network rhythmogenesis in a reduced Traub model for CA3 neurons. J Comput Neurosci 1:39–60.

Rockwood K, Beattie BL, Eastwood MR, Feldman H, Mohr E, Pryse-Phillips W, Gauthier S (1997) A randomized, controlled trial of linopirdine in the treatment of Alzheimer's disease. Can J Neurol Sci 24:140–145.

Romero M, Reboreda A, Sánchez E, Lamas JA (2004) Newly developed blockers of the M-current do not reduce spike frequency adaptation in cultured mouse sympathetic neurons. Eur J Neurosci 19:2693–2702.

Peters HC, Hu H, Pongs O, Storm JF, Isbrandt D (2005) Conditional transgenic suppression of M channels in mouse brain reveals functions in neuronal excitability, resonance and behavior. Nat Neurosci 8:51–60.

Storm JF (1990) Potassium currents in hippocampal pyramidal cells. Prog Brain Res 83:161–187.

Tiesinga PH, Fellous JM, José JV, Sejnowski TJ (2001) Computational model of carbachol-induced delta, theta, and gamma oscillations in the hippocampus. Hippocampus 11:251–274.

Traub RD, Bibbig A, Fisahn A, LeBeau FE, Whittington MA, Buhl EH (2000) A model of gamma-frequency network oscillations induced in the rat CA3 region by carbachol in vitro. Eur J Neurosci 12:4093–4106.

Traub RD, Draguhn A, Whittington MA, Baldeweg T, Bibbig A, Buhl EH, Schmitz D (2002) Axonal gap junctions between principal neurons: a novel source of network oscillations, and perhaps epileptogenesis. Rev Neurosci 13:1–30.

Traub RD, Pais I, Bibbig A, LeBeau FE, Buhl EH, Hormuzdi SG, Monyer H, Whittington MA (2003) Contrasting roles of axonal (pyramidal cell) and dendritic (interneuron) electrical coupling in the generation of neuronal network oscillations. Proc Natl Acad Sci U S A 100:1370–1374.

Vanner S, Evans RJ, Matsumoto SG, Surprenant A (1993) Potassium currents and their modulation by muscarine and substance P in neuronal cultures from adult guinea pig celiac ganglia. J Neurophysiol 69:1632-1644.

Vervaeke K, Gu N, Agdestein C, Hu H, Storm JF (2006) Kv7/KCNQ/M-channels in rat glutamatergic hippocampal axons and their role in regulation of excitability and transmitter release. J Physiol 576:235–256.

Williams JH, Kauer JA (1997) Properties of carbachol-induced oscillatory activity in rat hippocampus. J Neurophysiol 78:2631–2640.

Yue C, Yaari Y (2006) Axo-somatic and apical dendritic Kv7/M channels differentially regulate the intrinsic excitability of adult rat CA1 pyramidal cells. J Neurophysiol 95:3480–3495.